

## Suppressed accretion onto massive black hole binaries surrounded by thin disks

CHRISTOPHER TIEDE <sup>1</sup>, JONATHAN ZRAKE <sup>2</sup>, ANDREW MACFADYEN <sup>3</sup> AND ZOLTÁN HAIMAN <sup>4, 5</sup>

<sup>1</sup>*Niels Bohr Institute, Blegdamsvej 17, 2100 Copenhagen, Denmark*

<sup>2</sup>*Department of Physics and Astronomy, Clemson University, Clemson, SC 29634, USA*

<sup>3</sup>*Center for Cosmology and Particle Physics, Physics Department, New York University, New York, NY 10003, USA*

<sup>4</sup>*Department of Astronomy, Columbia University, New York, NY 10027, USA*

<sup>5</sup>*Department of Physics, Columbia University, New York, NY 10027, USA*

### ABSTRACT

We demonstrate that gas disks around binary systems might deliver gas to the binary components only when the circumbinary disk is relatively warm. We present new grid-based hydrodynamics simulations, performed with the binary on the grid and a locally isothermal equation of state, in which the binary is seen to functionally “stop accreting” if the orbital Mach number in the disk exceeds a threshold value of about 40. Above this threshold, the disk continues to extract angular momentum from the binary orbit, but it delivers very little mass to the black holes, and instead piles up mass in a ring surrounding the binary. This ring will eventually become viscously relaxed and deliver mass to the binary at the large-scale inflow rate. However we show that the timescale for such relaxation can far exceed the implied binary lifetime. We demonstrate that the ability of a binary-disk system to equilibrate is dependent on the efficiency at which accretion streams deposit mass onto the binary; which in turn is highly sensitive to the thermodynamic conditions of the inner disk. If disks around massive black hole binaries do operate in such non-accreting regimes, it suggests these systems may be dimmer than their single black hole counterparts, but could exhibit dramatic re-brightening after the black holes in-spiral and merge. This dimming occurs at high photon energies, corresponding to the effective truncation of the circumbinary disk. As a result, such system may be underluminous in UV bands and missing X-ray emission entirely, potentially resembling the spectra of ‘Little Red Dots’ recently identified in JWST observations.

*Keywords:* Accretion (14) — Active galactic nuclei(16) — Hydrodynamical simulations (767) — Supermassive black holes (1663)

### 1. INTRODUCTION

Modern cosmology predicts the frequent formation of super-massive black hole binaries (SMBHBs) following major galaxy mergers (Begelman et al. 1980; Volonteri et al. 2003; Dotti et al. 2007; Kormendy & Ho 2013). Many of these SMBHBs are expected to interact with gas that reaches the galactic center, much as single super-massive black holes do in ordinary active galactic nuclei (AGN) (Gaskell 1985; Barnes & Hernquist 1996). Periodic variability associated with the orbital motion of the binary is a potential signpost of accreting

binary massive black holes, and could thus facilitate the selection of SMBHB candidates in time-domain electromagnetic (EM) surveys (Komossa 2006; Graham et al. 2015; D’Orazio et al. 2015a; Charisi et al. 2016; Chen et al. 2020). SMBHBs might also be multi-messenger sources when they emit gravitational radiation in-band for pulsar timing experiments or future space-based interferometers such as LISA.

Early analytic work on binary accretion posited that tidal torques from the rotating potential would suppress or even halt mass flow onto the binary components (Pringle 1991; Milosavljevic & Phinney 2005; Liu & Shapiro 2010). Numerical simulations revealed that binaries do in fact expel material from their central region (Artymowicz & Lubow 1994, 1996; Cuadra et al. 2009; Shi et al. 2012), but that gas still falls onto the

binary via tidal streams (MacFadyen & Milosavljević 2008; Farris et al. 2014; Shi & Krolik 2015). It was subsequently demonstrated that the system can come into equilibrium where the accretion rate throughout the disk is constant and equal to that onto the binary (Rafikov 2016; Miranda et al. 2017; Muñoz et al. 2019).

The majority of the numerical work on accreting binaries considers disks with significant pressure support and aspect ratio  $h/r = 0.1$  (see Lai & Muñoz 2023 for review). Canonical disk modeling envisions however, that accretion disks around massive black holes are truly thin with  $h/r \sim 10^{-2} - 10^{-3}$  (Shakura & Sunyaev 1973). Ragusa et al. (2016) first treated thinner disks with smoothed particle hydrodynamics (SPH) and reported suppressed accretion rates. This was supported by studies of finite tori in Tiede et al. (2020) and Heath & Nixon (2020). Accretion quenching in colder systems was similarly observed for infinite disks by Dittmann & Ryan (2022), but they stressed that the suppression was a spurious artifact of the initial configuration; and that accurately approximating the flow of angular momentum in the disk restores a steady solution (see also Miranda et al. 2017; Dempsey et al. 2020).

The previous explorations on this topic still considered disks thicker than the canonical thin disk limit for  $h/r$  by a factor of a few. Here we report high-resolution grid-based hydrodynamics simulations approaching the truly thin-disk limit  $h/r \sim 10^{-2}$ , which — in conjunction with simple analytic modeling — show the existence of long-lived non-accreting phases. We also demonstrate that one can characterize such systems with a single parameter, the stream efficiency (referring to the likelihood that a gas parcel entering the tidally evacuated cavity around the binary falls onto one of the black holes). Our guiding physical understanding is laid out in Section 2, and the simulation setups are summarized in Section 3. We report on the dynamics of such truly thin disks in Section 4 and discuss the implications to electromagnetic searches for SMBHBs and future numerical studies in Section 5. We summarize our main conclusions in Section 6.

## 2. PHYSICAL PICTURE

A circumbinary disk (CBD) surrounds a binary of mass  $M$ , semi-major axis  $a$ , and orbital frequency  $\Omega_b$ . The large-scale rate of mass flow through the CBD is  $\dot{M}_\infty$ , and gas accretes to the binary components at rate  $\dot{M}_b$ . The time averaged rate  $\langle \dot{M}_b \rangle$  and  $\dot{M}_\infty$  are equal after a steady-state accretion flow is established.<sup>1</sup> We are considering circumbinary disks that may take a long

time to viscously relax, so we do not assume that  $\dot{M}_\infty$  and  $\dot{M}_b$  are equal a priori.

The time-varying tidal field of the binary deforms the innermost portions of the CBD, peeling away streams of gas. The streams pass near the black holes, delivering gas onto strongly interacting orbits at a rate  $\dot{M}_{\text{int}}$ . A fraction,  $\chi \equiv \dot{M}_b/\dot{M}_{\text{int}}$ , of the gas parcels lose orbital energy via self-collisions and are gravitationally captured onto orbits around one of the black holes. They then accrete through one of the circum-single disks called “minidisks”. We refer to this fraction  $\chi$  as the stream efficiency. The remaining gas parcels are tidally up-scattered in the encounter, and rejoin the CBD with their specific angular momentum increased by an amount on the order of  $a^2\Omega_b$ .

The gas-induced torque exerted on the binary through this process can be expressed as

$$\dot{J}_b = (\eta\dot{M}_b - \dot{M}_{\text{int}})a^2\Omega_b, \quad (1)$$

where  $\eta = M_1M_2/M^2$  is the symmetric mass-ratio. The first term is the accretion torque, and the second term is identified as the tidal torque associated with the rejected, up-scattered gas parcels. The accretion torque is negligible when most of the gas is rejected,  $\chi \ll 1$ . In that limit  $\dot{J}_b \simeq -\chi^{-1}\dot{M}_b a^2\Omega_b$ . We also define a dimensionless “torque parameter”,  $\ell_0 \equiv \dot{J}_b/(\dot{M}_b a^2\Omega_b)$ , representing the torque on the binary per unit accreted mass. If a very small fraction of the interacting gas is captured, then  $\ell_0 \simeq -1/\chi$ , and the quantity  $-\ell_0$  may then also be interpreted as the “recycling number”, meaning the number of times a gas parcel has a strong encounter with the binary before it falls into a black hole.<sup>2</sup>

When  $\chi \ll 1$  the binary interacts with the disk in a “non-accreting” phase. Such a phase would inevitably be temporary, as gas would continue to feed from the large-scale disk and accumulate in a dense “ring” of gas in the inner CBD. There would be a characteristic timescale  $t_{\text{eq}}$  for the ring to relax so that a balance is established where  $\langle \dot{M}_b \rangle \simeq \dot{M}_\infty$ .

We consider an accretion flow that cools and flattens at scales that are large compared to  $a$ . To estimate  $t_{\text{eq}}$ , we separate the disk into two zones: an inner zone (the ring) which has adjusted to the binary torque  $\dot{J}_b$ , and an outer zone which has not yet become “aware” of the inner binary torque (e.g. Kocsis et al. 2012; Rafikov 2016; Duffell et al. 2024; Zrake et al. 2024). The disk in the outer zone is formed from the large-scale accre-

<sup>1</sup>  $\langle \cdot \rangle$  denotes an average over a viscous time.

<sup>2</sup>  $\ell_0 > 0$  has been reported for some system parameters, which arises when  $\chi$  is a significant fraction of one. Accurately describing this limit would require an adjustment to our model, but in the  $\chi \ll 1$  regime,  $\ell_0 < 0$  always.

tion flow, and carries net-zero radial angular momentum current. The ring grows radially over time as the binary influence is communicated outwards (Syer & Clarke 1995; Ivanov et al. 1999). The radius at which the two zones meet is called the “radius of influence”, denoted as  $r_\nu(t)$ . The radius of influence is defined implicitly as  $t_{\text{visc}}(r_\nu(t)) = t$ , where  $t_{\text{visc}}(r) \equiv 2r^2/3\nu(r)$  is the viscous relaxation timescale at radius  $r$ , and the viscosity  $\nu(r)$  is parameterized explicitly as a function of radius.

The surface density radial profile in the ring, which is relaxed with respect to the torque parameter  $\ell_0$ , is

$$\Sigma(r, t) = \frac{\dot{M}(t)}{3\pi\nu(r)} \left( 1 - \ell_0 \frac{a^2\Omega_b}{j(r)} \right), \quad (2)$$

where  $j(r) = \sqrt{GM}r$  is the specific angular momentum of circular orbits at radius  $r$  and  $\dot{M}(t)$  is the mass flow through the ring, and onto the binary. The outer zone (beyond  $r_\nu$ ) maintains the initial configuration  $\Sigma_{\text{init}}(r) = \dot{M}_\infty/3\pi\nu(r)$ . The rate of mass flowing through the inner ring is obtained by imposing a matching condition at the radius of influence  $\Sigma(r_\nu) = \Sigma_{\text{init}}(r_\nu(t), t)$ ,

$$\begin{aligned} \dot{M}(t) &= \frac{\dot{M}_\infty}{1 - \ell_0 a^2\Omega_b/j_\nu(t)} \\ &= \frac{\dot{M}_\infty}{1 - \ell_0 \left(\frac{3}{2}\bar{\nu}\Omega_b t\right)^{-1/3}}, \end{aligned} \quad (3)$$

where  $j_\nu(t) \equiv \sqrt{GM}r_\nu(t)$  is the specific angular momentum at the radius of influence. On the second line we have inserted the  $\alpha$ -viscosity law  $\nu(r) = \bar{\nu}\sqrt{GM}r$  with  $\bar{\nu} \equiv \alpha(h/r)^2$ . For a more general viscosity prescription  $\nu(r) \propto r^n$ , the exponent 1/3 is changed to  $\lambda \equiv (4 - 2n)^{-1}$ . For a constant- $\nu$  viscosity law  $n = 0$  and  $\lambda = 1/4$ .

A family of accretion rate curves defined by Equation 3 is illustrated in Figure 1 for a range of values of  $\ell_0$  in an  $\alpha$ -disk. When  $\ell_0$  is large and negative,  $\dot{M}(t) \propto t^{1/3}$  as shown by the dashed blue line. When  $\ell_0$  is positive, the accretion rate is formally positive only at times  $t > 2/(3\bar{\nu}\Omega_b\ell_0^3)$ . In general this model is not expected to be accurate at very early times. In simulated disks, the early phase is seen to exhibit a complex adjustment phase lasting a fraction of a viscous time, as shown in Figure 2.

We note that circumbinary disks only permit mildly positive values of  $\ell_0 \lesssim \mathcal{O}(1)$ . If  $\ell_0$  exceeds this range, the density in the ring must approach zero in order to accommodate both the mass and angular momentum flow. This causes the disk to physically detach from the binary system (see Rafikov 2016). On the other hand, any value  $\ell_0 < 0$  is in principle permitted, and thus a

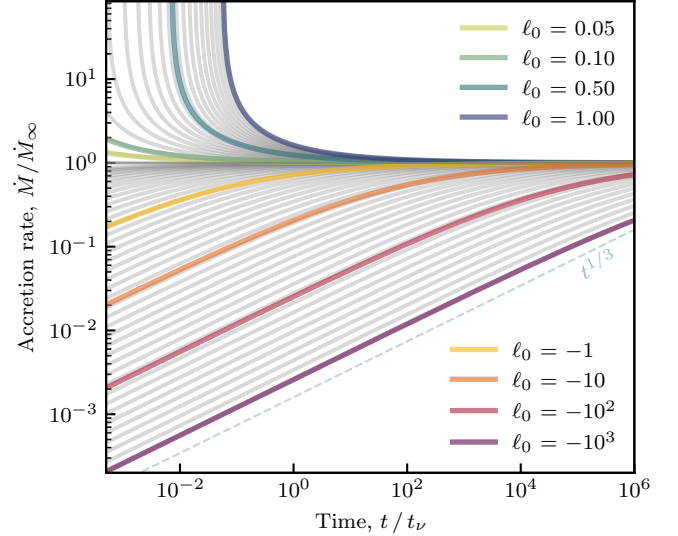


**Figure 1.** Family of curves for  $\dot{M}(t)$  from a zero-torque  $\alpha$ -disk for a given torque parameter  $\ell_0$ .  $t_\nu$  is the viscous time at  $r = a$ . The dashed-blue line illustrates the power law  $t^{1/3}$  growth for an alpha viscosity model in a non-accreting phase.

non-accreting phase can be long-lived. Equation 3 can be inverted to express the time required to achieve some accretion rate  $\dot{M}$ ,

$$t(\dot{M}) = \frac{P_b}{3\pi\bar{\nu}} \left( \frac{1 - \dot{M}_\infty/\dot{M}}{\ell_0} \right)^{-1/\lambda}, \quad (4)$$

where  $P_b$  is the binary period. Thus the time required for the disk to equilibrate, i.e. for accretion to “turn on”, depends strongly on the torque parameter  $\ell_0$ , or equivalently on the stream efficiency  $\chi$ . In terms of  $\chi$ ,  $t_{\text{eq}} \propto \chi^{-3}$  for the  $\alpha$ -viscosity law and  $t_{\text{eq}} \propto \chi^{-4}$  for the constant- $\nu$  viscosity law.

### 3. SIMULATION SETUPS

We solved the vertically averaged Navier-Stokes equations for the evolution of a thin gas disk around a circular, equal-mass binary with the finite-volume code *Sailfish* (Zrake & MacFadyen 2024). The disk is geometrically thin with characteristic scale height  $h \ll r$ . The gas is locally isothermal with orbital Mach number  $\mathcal{M} \equiv (h/r)^{-1}$ . The disk internal stresses are modeled using the  $\alpha$ -viscosity law,  $\nu = \alpha c_s h$  where  $c_s$  is the local sound speed and  $\alpha \lesssim 1$ .

The fiducial setup is essentially the “standard” binary-disk setup described in Duffell et al. (2024), with surface density modified by a factor  $\sqrt{a/r}$  to accommodate an  $\alpha$ -viscosity law. We additionally explore a set of initial surface densities with large inner pile-ups, detailed in Section 4.2. The gas orbits are initially circular and Keplerian. Note that in that standard setup with  $\mathcal{M} = 10$

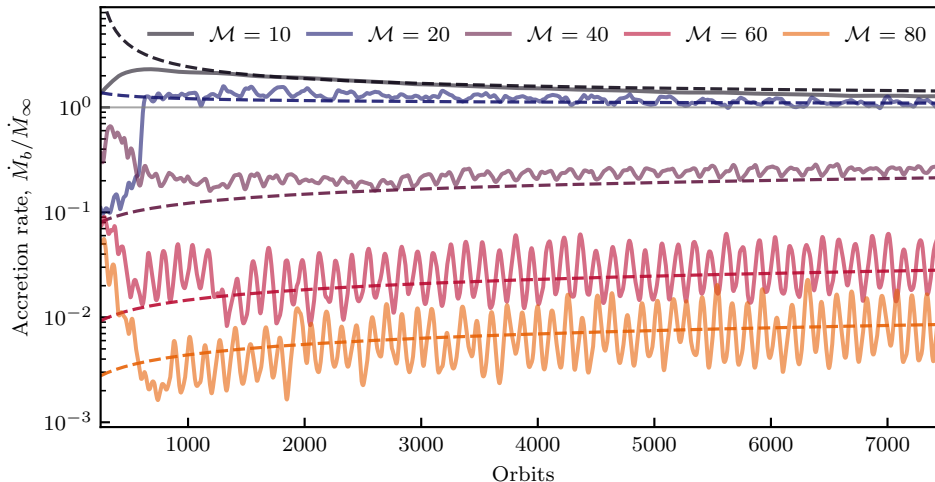


**Figure 2.** Accretion rates for each system from the “standard” setup. Dashed lines are from the analytic expression for  $\dot{M}(t)$  from Equation 3. The torque parameter is determined empirically as  $\ell_0 = \{0.59, 0.17, -7.05, -66.13, -224.22\}$  (in order of growing  $\mathcal{M}$ ) from averages over a viscous time ( $\sim 4 \times 10^3$  orbits at the cavity edge). We note that the  $\mathcal{M} = 80$  run is not a converged result (as will be shown in Figure 4), but that the accretion rate is still fully consistent with the measurement of  $\ell_0$  at this resolution.

and  $\nu = 10^{-3} a^2 \Omega_b$ , the gas-induced binary torque is positive, and the accretion rate overshoots the inflow rate  $\dot{M}_\infty$  while the disk relaxes from a zero-torque configuration. In scenarios where the gas-induced binary torque is negative, we expect the opposite effect, as discussed in Section 2. The outer boundary condition is enforced by use of a buffer region, wherein the velocity and surface density fields are driven exponentially toward the initial condition (see e.g. Westernacher-Schneider et al. 2022).

Accretion onto the binary components is modeled by the use of “sink” regions surrounding the binary components. We use the torque-free sink prescription as described in Dempsey et al. (2020) (see also Dittmann & Ryan 2021), with the sink radius set to  $r_{\text{sink}} = 0.05a$  ( $r_{\text{sink}}$  is also used as the gravitational softening radius).

We explore solutions for increasingly cold disks with Mach numbers  $\mathcal{M} = \{10, 20, 40, 60, 80, 100\}$ . We vary  $\alpha$  commensurately to fix  $\bar{\nu} = 10^{-4}$ . This yields values  $\alpha = \{0.01, 0.04, 0.16, 0.36, 0.64, 1.0\}$ , respectively. The viscous timescale is thus the same across runs with various Mach numbers. The simulation domain is a square with side length  $24a$ . To probe numerical convergence, the grid resolution is varied for each run in the range of  $\Delta x = 0.004a - 0.01a$ .

## 4. RESULTS

### 4.1. The non-accreting phase

Figure 2 shows the accretion rates for the standard systems evolved at resolution  $\Delta x = 0.01a$  for approximately two viscous times at the cavity edge  $\gtrsim 8000$  orbits. We observe that this configuration yields a quasi-steady configuration for the  $\mathcal{M} \leq 20$  systems, but that

all other solutions are still in a non-accreting phase with  $\dot{M}_b \ll \dot{M}_\infty$ . We additionally include the analytic estimate from Equation 3 (where we have taken  $\dot{M} = \dot{M}_b$ ) as dashed lines of the same color, with  $\ell_0$  determined empirically as  $\langle \dot{J}_b \rangle / (\langle \dot{M}_b \rangle a^2 \Omega_b)$ . We find that Equation 3 captures the normalization and evolution of  $\dot{M}_b$  remarkably well for both the over- and under-accreting systems. Use of Equation 4 and the measured values of  $\ell_0$  imply that the  $\mathcal{M} = 40$  system would require  $\mathcal{O}(10^5)$  orbits to reach  $\dot{M}_b = 0.5\dot{M}_\infty$ , while the  $\mathcal{M} = 80$  system would require  $\mathcal{O}(10^{10})$  orbits.

### 4.2. Steady-states

Given sufficient time and mass, any disk-binary system will ultimately achieve a steady-state. However Equation 4 shows that it could be prohibitive to run a simulation to  $t_{\text{eq}}$ . Nevertheless, a simulation can be prepared near a steady state by initializing the CBD with the surface density profile in Equation 2 and guessing the torque parameter  $\ell_0$  (Miranda et al. 2017; Dempsey et al. 2020; Dittmann & Ryan 2022).

It turns out the torque parameter can be accurately measured even when the system is not in a steady state. This is a main result and is detailed in the following section (Section 4.3). At a higher resolution  $\Delta x = 0.008a$ , we measured  $\ell_0$  from the standard setup over a viscous time. We then started new simulations for  $\mathcal{M} \geq 40$  with these values of  $\ell_0$ . We denote this set of initial conditions as  $\Lambda$ . Starting from  $\Lambda$ , after the start-up transient we observed the binary to accrete in a statistical steady-state with  $\langle \dot{M}_b(t) \rangle \simeq \dot{M}_\infty$  and  $\dot{J}_b / (\dot{M}_b a^2 \Omega_b) \simeq \text{const}$ ,

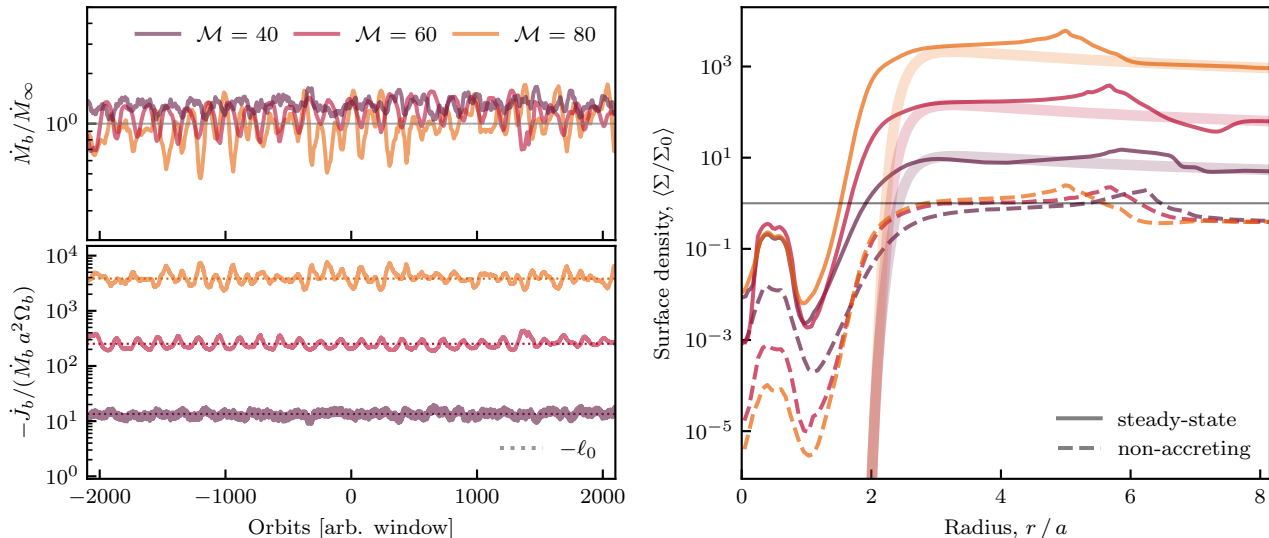


**Figure 3.** (Left) Time-series of an arbitrary window of the binary accretion rate and torque per accreted mass in an approximate steady-state. The dotted lines denote the measured torque parameter,  $-\ell_0$ . (Right) The average surface density profiles from the steady-state phase in solid, and the non-accreting phase in dashed.  $\Sigma_0$  is the characteristic disk density  $\dot{M}_\infty / 3\pi\bar{\nu}$ , and the initial profiles for the steady-state runs are illustrated by the faint bands of equivalent color.

as seen in the left panels of Figure 3. The dotted line illustrates the associated value  $-\ell_0$ .

The right panel of Figure 3 shows the average surface density profiles from both the non-accreting phase (dashed lines; Section 4.1) and the steady-state phase (solid lines) in units of the characteristic disk density  $\Sigma_0 = \dot{M}_\infty / 3\pi\bar{\nu}$ . The faint bands illustrate the initial profiles for the steady-state runs. The equilibrium mini-disk density also appears insensitive to  $\mathcal{M}$  (similarly observed in Tiede et al. 2020). This is possibly because it adjusts itself to accommodate  $\dot{M}_\infty$ , and thus, is sensitive to viscosity  $\nu(\alpha)$ , but not  $\mathcal{M}$ . Conversely, in the non-accreting phases the minidisks are starved with surface densities proportional to  $\dot{M}_b$ .

#### 4.3. Self-similar evolution

We stress that the results of Sections 4.1 and 4.2 represent two phases of evolution for the same systems. The former a transient (albeit potentially long-lived) phase as the disk adjusts to angular momentum injection from the binary, and the latter the equilibrium configuration which persists either until the outer gas reservoir is depleted or the binary merges.

It is not self-evident that the stream efficiency, and in turn  $\ell_0$ , is insensitive to the varying gas distribution (e.g. Figure 3, right). However, we find that when  $\chi$  is small, this is the case and that  $\chi \simeq -\ell_0^{-1}$  is generally a fixed property of the system (i.e. does not change over time as the system equilibrates). Figure 4 shows the stream efficiency (top panel) determined as  $\chi = \ell_0^{-1}$  from the results of both Sections 4.1 and 4.2. Because these had

different resolutions, we supplement each with 2000 orbits of their complimentary simulations. Namely, *dashed lines* denote systems initialized in the standard setup, and *solid lines* those with initial condition set  $\Lambda$  (from Section 4.2). We additionally include “upsampled” solutions that have had their resolution doubled and evolved for an additional few hundred orbits. To emphasize how the solid- and dashed-lines symbolize dramatically dissimilar accretion states, the bottom panel of Figure 4 shows the associated accretion rates. The stream efficiency and torque parameter are insensitive (at leading order) to the mass distribution and to whether the binary is overfed, starved, or in steady-state.

The critical feature for determining  $\chi$  is the system resolution. The growing separation between solid-dashed pairs in the top panel also indicates a lack of numerical convergence. Until the simulation is numerically converged,  $\chi$  decreases monotonically with increasing resolution.<sup>3</sup> Generally,  $\chi$  decays extremely rapidly with disk temperature, and as one approaches the continuum limit the stream efficiency can become as low as  $\chi < 10^{-5}$  as  $\mathcal{M} \rightarrow 100$ . We thus expect that  $\chi$  would be lower than  $10^{-5}$  in a numerically converged run of a truly thin disk with  $\mathcal{M} \sim 100 - 1000$ , and we conclude that circumbinary black hole accretion disks in nature might persist in non-accreting configurations over timescales exceeding the binary lifetime.

<sup>3</sup> We plan to present a detailed model for mass capture from the CBD onto binary minidisks that accounts for this behavior in forthcoming work.

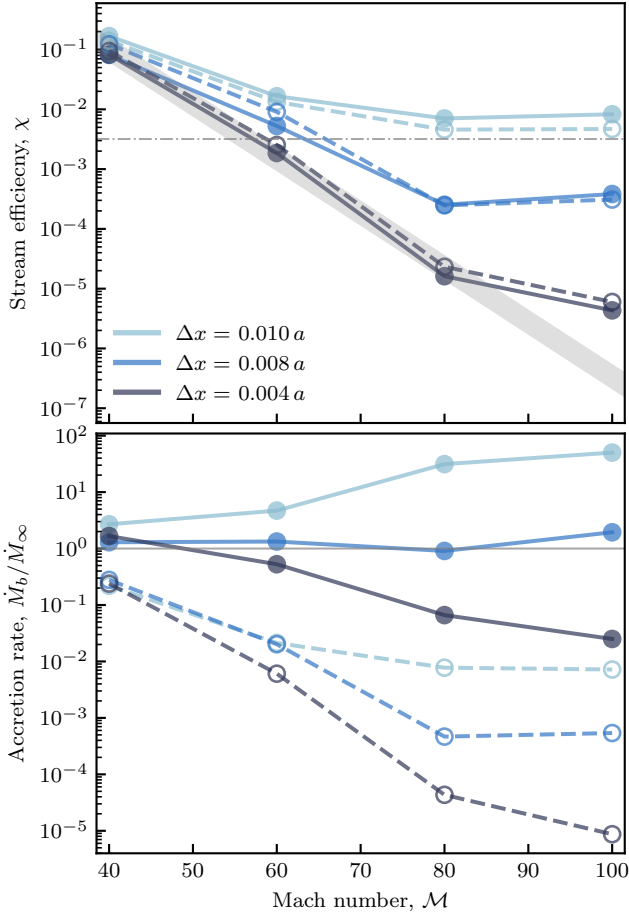


**Figure 4.** Stream efficiency  $\chi \approx \ell_0^{-1}$  (top) and accretion rate (bottom) as a function of Mach number and resolution. Dashed lines denote the “standard” initial disk configuration (Duffell et al. 2024). The solid lines indicate initial condition set  $\Lambda$ , which permitted a steady-state at  $\Delta x = 0.008 a$ .  $\dot{M}_b$  is sensitive to the surface density profile of the system but  $\chi$  is not. The dashed-dotted line denotes the condition from Equation 7 below which a binary will merge before accreting significantly. The light-grey band illustrates the exponential function  $\chi(\mathcal{M})$  in Section 5.1.

## 5. DISCUSSION

### 5.1. Observational Implications

*Binary lifetimes*—We have demonstrated that massive binaries embedded in realistically thin disks may undergo sustained phases of negligible accretion. Despite the truncation of the mass flow in the non-accreting phase, gas parcels continue to interact with the binary removing angular momentum with each strong encounter. To accommodate the sustained injection of angular momentum, the mass of the inner ring grows with time. The characteristic timescale for the binary to merge then is  $t_m \sim M/\dot{M}_\infty$ , that required for the disk to supply an equivalent binary mass to the inner-

ring. For a disk with  $\dot{M}_\infty$  taken as the Eddington rate, this is a Salpeter time  $t_{\text{sal}} \simeq 4.5 \times 10^7$  years. To compare with  $t_{\text{eq}}$ , we consider  $\chi(\mathcal{M})$  as a simple decaying function  $k_0 e^{-k_1 \mathcal{M}}$ . This relation is shown in Figure 4 as a light grey band for  $k_0 = 440$  and  $k_1 = 0.21$ . For thin, radiatively efficient (isothermal) accretion, this is likely a conservative estimate as we anticipate the dependence to steepen as resolution is increased. One can readily see that the decaying  $\chi(\mathcal{M})$  causes  $t_{\text{eq}}$  to rapidly overtake  $t_{\text{sal}}$  with growing Mach number. Because the “turn on” time is dominated by this relation, it can be approximated as

$$t_{\text{eq}} \simeq 1.3 \times 10^{14} \left( \frac{P_b}{1 \text{ yr}} \right) \times \exp \left[ 0.6 \left( \frac{\mathcal{M}_{3a}}{80} \right) \right] \text{ yr} \quad (5)$$

where

$$\mathcal{M}_{3a} \simeq 80 \left( \frac{\alpha}{0.005} \right)^{1/10} \left( \frac{f_{\text{Edd}}}{1.0} \right)^{-1/5} \left( \frac{P_b}{1 \text{ yr}} \right)^{-1/30} \left( \frac{M}{10^5 M_\odot} \right)^{2/15}$$

is the Mach number in the inner ring ( $r = 3a$ ) in a gas-pressure dominated disk with primary opacity from electron scattering accreting at  $\dot{M}_\infty$  equal to  $f_{\text{Edd}}$  times the Eddington rate.

*Electromagnetic searches*—Such suppressed accretion phases and severe “turn on” times could pose challenges for searches for compact massive binaries in electromagnetic surveys. One of the primary search techniques is to identify periodic emission features tied to the underlying binary period. The hydrodynamic component of such periodicity is typically connected with the binary accretion rate (e.g. Farris et al. 2014; D’Orazio et al. 2015a; Combi et al. 2022; Westernacher-Schneider et al. 2022). The most prominent variability is also expected to be associated with higher energy emission (like in X-rays or the UV) from the binary minidisks (Cochiararo et al. 2024). These components may not in fact be present however, under sustained suppression of the binary accretion rate and the associated starvation of the minidisks. Alternative search methods based on the periodic lensing or boosting of emission from material co-moving with the binary components (D’Orazio et al. 2015b; D’Orazio & Di Stefano 2018; Davelaar & Haiman 2022) are also likely to be compromised in the absence of persistent minidisks.

Variability at lower frequencies (e.g. in the optical or infrared) is typically associated with features in the inner disk (Westernacher-Schneider et al. 2022) and may yet be present during non-accreting phases (infrared variability may also come from reverberation D’Orazio & Haiman 2017). However, the truncation of the flow against the binary tidal barrier at  $\sim \text{few} \times a \gg GM/c^2$ ,

as opposed to near the inner most stable circular orbits may considerably lower the total luminosity of such sources. The luminosity suppression will be of order  $a/r_g$  where  $r_g = GM/c^2$  is the gravitational radius. For massive binaries with month-to-year long orbital periods, this is  $a/r_g \sim \mathcal{O}(10^2 - 10^4)$  which could make binaries with truly thin disks meaningfully dimmer and harder to discover than their single-BH AGN-counterparts.

That said, regardless of whether the system “turns-on” or not, a reservoir of mass approximately equal to that of the binary will be released following a GW-driven merger. This could instantiate periods of high-Eddington accretion in a “dam-break” scenario and cause the post-merger black hole to light up as a luminous quasar (Milosavljevic & Phinney 2005; Shapiro 2010; Tanaka et al. 2010).

*Little red dots*—JWST deep fields have recently revealed an enigmatic population of high-redshift galaxies dubbed “Little Red Dots” (LRDs; Matthee et al. 2024). LRDs appear very compact and are comparatively abundant relative to the previously known population of high- $z$  AGN (Labbé et al. 2023). Around 60% of these sources possess distinct broad emission lines, a tell-tale feature of Type-1 AGN, suggesting a central SMBH as their origin.<sup>4</sup> From the broad lines, the central masses are estimated to be  $M \sim 10^6 - 10^9 M_\odot$  (Maiolino et al. 2023; Harikane et al. 2023; Greene et al. 2024). Compared to the previously known population of high-redshift AGN, LRDs have lower UV luminosities at comparable black hole mass, and they show almost no evidence for X-ray emission (Kocevski et al. 2024). The observed spectrum has been challenging to explain with typical reddening, and the lack of X-rays seems to necessitate unconventional AGN configurations (Yue et al. 2024; Pacucci & Narayan 2024).

Suppressed accretion associated with a truly thin disk around a massive binary may however reproduce such features. If the system preserves the broad line regions in the outer disk, the truncation of the disk from a binary’s tidal torques could result in a suppression of higher energy emission from the disk’s inner-regions. Assuming thermal emission from the disk and that most of the light radiated at frequency  $f$  is emitted at the radius where  $kT(r) \sim hf$ , emission will start being suppressed at frequencies where  $r(f) \approx a$  (Roedig et al. 2014). The char-

acteristic temperature of an untruncated disk at such radii would be

$$T_a = \left( \frac{3}{8\pi\sigma} \frac{GM\dot{M}}{a^3} \right)^{1/4} \quad (6)$$

$$\simeq 7700 \left( \frac{f_{\text{Edd}}}{1.0} \cdot \frac{M}{5 \times 10^7 M_\odot} \right)^{1/4} \left( \frac{P_b}{1 \text{ yr}} \right)^{-1/2} \text{ K}$$

such that the removal of said regions in a truncated disk would start censoring emission in the near-UV. The associated starvation of the minidisks would additionally eliminate the hottest regions of the flow near the BH horizons that would typically emit X-rays.

The observed redshifts of LRDs  $4 < z < 8$  also align with more gas-rich epochs where one might particularly expect massive binaries to evolve through gaseous environments, and the number density of major galaxy mergers at  $z \sim 6$  could be high enough to match that of LRDs (Greene et al. 2024). The number density of binaries with periods that do not suppress these systems’ optical emission, however, may pose a challenge. We believe this warrants a more detailed examination, and plan to explore the extent to which such truncated flows could account for the observed properties of LRDs in future work.

## 5.2. Numerical modeling and future directions

As noted in the Introduction, comparatively mild suppression of the binary accretion rate in increasingly cold disks had previously been observed in both finite volume and SPH studies. However, it had either been attributed to an associated decrease in the strength of viscous torques or regarded as a spurious manifestation of a poorly tuned initial condition. We have demonstrated not only that non-accreting phases can be long-lived relative to the binary lifetime, but that they occur at fixed viscous strengths.

Such non-accreting phases occur because the efficiency of mass capture from streams drops rapidly with decreasing disk temperature (Section 2). However, we have determined that  $\chi$  is insensitive to the system state, and only depends on the hydrodynamic properties of the disk and resolution. This is consistent with the observation in the literature that  $\dot{J}_b(t)/\dot{M}_b(t)$  seemingly always equilibrates to a stable value (close to the steady-state solution) in a viscous time or less; even in the presence of a time-evolving gas distribution and accretion rate (e.g. because of a finite disk that is being depleted Muñoz et al. 2020; Tiede et al. 2020; Penzlin et al. 2022).

From Figure 4 and Section 2 it is clear that the accretion rate, equilibration time, steady-state angular momentum current, and equilibrium gas-morphology are

<sup>4</sup> The primary alternative interpretation is that LRDs are very massive, compact, star-forming galaxies; but they would require unprecedentedly high stellar densities and their abundance would possibly be in tension with  $\Lambda$ CDM (Kocevski et al. 2023; Boylan-Kolchin 2023).

highly sensitive to the temperature of the circumbinary material, and particularly of the material that strongly interacts with the binary in streams. Thus, each of these quantities could in turn vary sensitively with physics that alter the inner disk vertical structure and thermodynamics. This may include a full treatment of heat injection and cooling mechanisms (see e.g. Westernacher-Schneider et al. 2022; Wang et al. 2023; Cocchiararo et al. 2024), binary eccentricity (Zrake et al. 2021; D’Orazio & Duffell 2021; Siwek et al. 2023), the inclusion of magnetic fields (c.f. Shi & Krolik 2015; Hopkins et al. 2024; Most & Wang 2024), or radiative effects (del Valle & Volonteri 2018; Williamson et al. 2022) in such truly thin conditions. Moreover, while treating the problem in two dimensions may well be valid for such thin solutions, warm circumbinary disks studied in 3D typically possess less eccentric and smaller cavities (e.g. Shi et al. 2012; Shi & Krolik 2015; Moody et al. 2019; Duffell et al. 2024; Most & Wang 2024). These are more closely attached to the binary and may permit larger stream efficiencies, even in such cold, isothermal solutions.

One can compute a general stream efficiency below which a binary will merge before it “turns on” (i.e.  $\dot{M}_b = 0.1\dot{M}_\infty$ ) by equating  $t_{\text{eq}}$  and  $t_{\text{sal}}$ . This yields a critical value ,

$$\chi_c \simeq 0.003 \left( \frac{\bar{\nu}}{10^{-4}} \right)^{-1/3} \left( \frac{P_b}{1 \text{ yr}} \right)^{1/3}. \quad (7)$$

This condition is illustrated as a dashed-dotted line in the top-panel of Figure 4. For shorter initial periods, the gravitational wave inspiral time also generally becomes shorter than  $t_{\text{eq}}$ . Quantifying how additional physics may alter the inner mass flow, stream capture dynamics, and in turn the equilibrium angular momentum current, then, will be crucial for more reliably determining the feasibility of discovering compact massive binaries as multi-messenger sources and for accurately determining their associated characteristics.

## 6. SUMMARY

We have studied the dynamics of massive binaries accreting from disks approaching the truly thin limit,  $\mathcal{M} \rightarrow 100$ . We have determined that such systems are highly inefficient at delivering mass to the binary, and as a result may undergo exceptionally long-lived non-accreting phases. We find that the time evolution

of such systems can be well described with a simple one-parameter model where the critical quantity is the stream efficiency  $\chi$ . This sets the characteristic equilibration time for the system, the equilibrium angular momentum current in the disk, and the associated steady-state density distribution.

Moreover, we have shown that  $\chi$  is an intrinsic property of the system which does not vary (to leading order) with the system accretion state or gas distribution. It is, however, highly sensitive to numerical spatial resolution. For gas conditions where we were unable to obtain numerically converged measures of  $\chi$ , it trends toward smaller values with increasing grid resolution, indicating that our simulations have only set upper bounds on  $\chi$  as a function of Mach number. As a result, we posit that if disks around massive binaries are well described by such a truly thin, isothermal configuration, then they may undergo substantial phases of limited or no accretion. This may severely limit the prospects for discovering such systems in electromagnetic surveys. It is important to mention that our estimates for the duration of non-accreting phases might only be accurate when the accretion flow forms an extended disk around the binary; if instead low-angular momentum gas were to fall more directly toward the binary, it might cause the formation of a dense ring of gas that could be accreted more promptly.

Lastly, we have determined that the stream efficiency and all subsequent properties of the system are exceptionally sensitive to the thermodynamic conditions of the inner disk. It is crucial both for modeling of SMBHB populations, and for the identification of SMBHB candidates from time-domain EM surveys, to understand whether realistically cold circumbinary disks exhibit such low stream efficiencies when additional physics are included.

- 1 C.T. sincerely thanks Daniel J. D’Orazio for useful and
- 2 illuminating discussions. This work was supported by
- 3 the European Union’s Horizon 2023 research and in-
- 4 novation program under Marie Skłodowska-Curie grant
- 5 agreement No. 101148364, by Sapere Aude Starting
- 6 grant No. 121587 through the Danish Independent Re-
- 7 search Fund, by the LISA Preparatory Science Pro-
- 8 gram (LPS) through NASA grant 80NSSC24K0440, and
- 9 by NASA Astrophysics Theory Program (ATP) grant
- 10 80NSSC22K0822.

## REFERENCES



- Barnes J. E., Hernquist L., 1996, *ApJ*, 471, 115
- Begelman M. C., Blandford R. D., Rees M. J., 1980, *Nature*, 287, 307
- Boylan-Kolchin M., 2023, *Nature Astronomy*, 7, 731
- Charisi M., Bartos I., Haiman Z., Price-Whelan A. M., Graham M. J., Bellm E. C., Laher R. R., Márka S., 2016, *MNRAS*, 463, 2145
- Chen Y.-C., et al., 2020, *MNRAS*, 499, 2245
- Cocchiararo F., Franchini A., Lupi A., Sesana A., 2024, *arXiv e-prints*, p. [arXiv:2402.05175](#)
- Combi L., Lopez Armengol F. G., Campanelli M., Noble S. C., Avara M., Krolik J. H., Bowen D., 2022, *ApJ*, 928, 187
- Cuadra J., Armitage P. J., Alexander R. D., Begelman M. C., 2009, *MNRAS*, 393, 1423
- D’Orazio D. J., Di Stefano R., 2018, *MNRAS*, 474, 2975
- D’Orazio D. J., Duffell P. C., 2021, *ApJL*, 914, L21
- D’Orazio D. J., Haiman Z., 2017, *MNRAS*, 470, 1198
- D’Orazio D. J., Haiman Z., Duffell P., Farris B. D., MacFadyen A. I., 2015a, *MNRAS*, 452, 2540
- D’Orazio D. J., Haiman Z., Schiminovich D., 2015b, *Nature*, 525, 351
- Davelaar J., Haiman Z., 2022, *PhRvL*, 128, 191101
- Dempsey A. M., Muñoz D., Lithwick Y., 2020, *ApJL*, 892, L29
- Dittmann A. J., Ryan G., 2021, *ApJ*, 921, 71
- Dittmann A. J., Ryan G., 2022, *MNRAS*, 513, 6158
- Dotti M., Colpi M., Haardt F., Mayer L., 2007, *MNRAS*, 379, 956
- Duffell P. C., et al., 2024, *arXiv e-prints*, p. [arXiv:2402.13039](#)
- Farris B. D., Duffell P., MacFadyen A. I., Haiman Z., 2014, *ApJ*, 783, 134
- Gaskell C. M., 1985, *Nature*, 315, 386
- Graham M. J., et al., 2015, *MNRAS*, 453, 1562
- Greene J. E., et al., 2024, *ApJ*, 964, 39
- Harikane Y., et al., 2023, *ApJ*, 959, 39
- Heath R. M., Nixon C. J., 2020, *A&A*, 641, A64
- Hopkins P. F., et al., 2024, *The Open Journal of Astrophysics*, 7, 19
- Ivanov P. B., Papaloizou J. C. B., Polnarev A. G., 1999, *MNRAS*, 307, 79
- Kocevski D. D., et al., 2023, *ApJL*, 954, L4
- Kocevski D. D., et al., 2024, *arXiv e-prints*, p. [arXiv:2404.03576](#)
- Kocsis B., Haiman Z., Loeb A., 2012, *MNRAS*, 427, 2660
- Komossa S., 2006, *Mem. Soc. Astron. Italiana*, 77, 733
- Kormendy J., Ho L. C., 2013, *ARA&A*, 51, 511
- Labbé I., et al., 2023, *Nature*, 616, 266
- Lai D., Muñoz D. J., 2023, *ARA&A*, 61, 517
- Liu Y. T., Shapiro S. L., 2010, *PhRvD*, 82, 123011
- MacFadyen A. I., Milosavljević M., 2008, *ApJ*, 672, 83
- Maiolino R., et al., 2023, *arXiv e-prints*, p. [arXiv:2308.01230](#)
- Matthee J., et al., 2024, *ApJ*, 963, 129
- Milosavljevic M., Phinney E. S., 2005, *The Astrophysical Journal Letters*, 622, L93
- Miranda R., Muñoz D. J., Lai D., 2017, *MNRAS*, 466, 1170
- Moody M. S. L., Shi J.-M., Stone J. M., 2019, *The Astrophysical Journal*, 875, 66
- Most E. R., Wang H.-Y., 2024, *arXiv e-prints*, p. [arXiv:2408.00757](#)
- Muñoz D. J., Miranda R., Lai D., 2019, *ApJ*, 871, 84
- Muñoz D. J., Lai D., Kratter K., Miranda R., 2020, *ApJ*, 889, 114
- Pacucci F., Narayan R., 2024, *arXiv e-prints*, p. [arXiv:2407.15915](#)
- Penzlin A. B. T., Kley W., Audiffren H., Schäfer C. M., 2022, *A&A*, 660, A101
- Pringle J. E., 1991, *MNRAS*, 248, 754
- Rafikov R. R., 2016, *ApJ*, 827, 111
- Ragusa E., Lodato G., Price D. J., 2016, *MNRAS*, 460, 1243
- Roedig C., Krolik J. H., Miller M. C., 2014, *ApJ*, 785, 115
- Shakura N. I., Sunyaev R. A., 1973, *A&A*, 24, 337
- Shapiro S. L., 2010, *PhRvD*, 81, 024019
- Shi J.-M., Krolik J. H., 2015, *ApJ*, 807, 131
- Shi J.-M., Krolik J. H., Lubow S. H., Hawley J. F., 2012, *ApJ*, 749, 118
- Siwek M., Weinberger R., Hernquist L., 2023, *MNRAS*,
- Syer D., Clarke C. J., 1995, *MNRAS*, 277, 758
- Tanaka T., Haiman Z., Menou K., 2010, *AJ*, 140, 642
- Tiede C., Zrake J., MacFadyen A., Haiman Z., 2020, *ApJ*, 900, 43
- Volonteri M., Haardt F., Madau P., 2003, *ApJ*, 582, 559
- Wang H.-Y., Bai X.-N., Lai D., 2023, *ApJ*, 943, 175
- Westernacher-Schneider J. R., Zrake J., MacFadyen A., Haiman Z., 2022, *PhRvD*, 106, 103010
- Williamson D. J., Bösch L. H., Hönig S. F., 2022, *MNRAS*, 510, 5963
- Yue M., Eilers A.-C., Ananna T. T., Panagiotou C., Kara E., Miyaji T., 2024, *arXiv e-prints*, p. [arXiv:2404.13290](#)
- Zrake J., MacFadyen A., 2024, *Sailfish: GPU-accelerated grid-based astrophysics gas dynamics code*, *Astrophysics Source Code Library*, record ascl:2408.004
- Zrake J., Tiede C., MacFadyen A., Haiman Z., 2021, *The Astrophysical Journal Letters*, 909, L13
- Zrake J., Clyburn M., Feyan S., 2024, *Changing-Look Inspirals: Trends and Switches in AGN Disk Emission as Signposts for Merging Black Hole Binaries*, In preparation
- del Valle L., Volonteri M., 2018, *MNRAS*, 480, 439